MESOSCALE ATMOSPHERIC CIRCULATION AND TRANSPORT OF COAGULATING AEROSOL OVER BRATSK-CITY

A.E. Aloyan, V.O. Arutyunyan, A.A. Lushnikov, and I.A. Zagainov

Institute of Computational Mathematics, Russian Academy of Sciences, Moscow
L.Ya. Karpov Physical Chemical Institute, Moscow
Received April 9, 1997

Atmospheric aerosol transport by air masses is studied using a model that accounts for the factors that may influence the particle size distribution. Among those factors there are the turbulent diffusion, atmospheric hydrothermodynamics, orography, disposition of aerosol emission sources, and particle growth due to coagulation. First we formulate a system of basic model equations and then the algorithm for its numerical solution. The model constructed has been used to reproduce the situation with the aerosol pollution of the atmosphere over Bratsk city in summer. Numerical calculations of submicron and fine aerosol fractions concentration were compared with the measurement data acquired in different parts of the city during a two-week mission in summer of 1990.

1. INTRODUCTION

Recently, a number of numerical models have been developed to treat the spread of impurities in the atmosphere (see Refs. 8, 10, 14, 19, and others). Although these models successfully explain many features of the passive impurity transport in the mesoscale atmospheric boundary layer, more elaborate models are still needed to provide for more reliable results that would allow for changes in the aerosol size spectra. However, there is a physical constraint on the model accuracy and it is the stochasticity of the processes influencing the atmospheric dynamics. As a consequence, aerosol particle size-distribution is formed by the inherently random factors so that it can never be reproduced even if the measurements are being carried out many times at the same point and under the absolutely identical conditions. So, a no less important question arises on to what extent it could be reasonable to modify the dynamic models of the atmospheric aerosol.

In this paper we describe a realistic model for estimating the contribution of anthropogenic factor to the aerosol pollution of the atmosphere. The following processes are involved in the model consideration.

Aerosol is transported by air flows. The reconstruction of the air flow velocity field is done numerically by solving the system of hydrothermodynamic equations with the account of some non-adiabatic factors, balance equations for turbulent energy and dissipation, and so on. Aerosol is transported as a passive impurity, that means that each aerosol particle moves in along-flow direction only. Particles are assumed to grow in size due to coagulation. Local sources of aerosol are also involved into the consideration.

Along with the main problem of aerosol transport in the atmosphere we deal, in this study, with some related tasks. For instance, we study the role of aerosol emissions in formation of the aerosol pollution of individual localities. To determine optimal arrangement of industrial pollution sources that could provide for the lowest possible air pollution, we study the processes of aerosol dispersal.

2. BASIC EQUATIONS

Below we formulate the complete set of equations needed to describe aerosol transport in the atmosphere. As was mentioned in the Introduction, aerosol particles are assumed passive, constrained to move strictly in along-flow directions of the hydrodynamic flux, formed by the atmospheric thermodynamic state and orography. The aerosol size-spectrum and number density are assumed to be affected by atmospheric turbulence and coagulation.

2.1. Equation of discontinuity

Here we present the model, developed in Ref. 9, which takes into account the transport and coagulation of atmospheric aerosol. The starting point of our approach is the discontinuity equation, which describes transport of a passive impurity denoted as $\varphi_i(\mathbf{r}, t)$

$$\frac{\partial \varphi_i}{\partial t} + \operatorname{div} \mathbf{u}\, \varphi_i = F_i(\varphi_i, x, y, z, t), \qquad (1)$$

where $\mathbf{u}$ is the vector of the flow velocity. The right-hand side of (1), being a functional of φ_i, includes terms describing sources, sinks, and chemical interactions among pollutants, as well as other factors influencing their concentrations.

0235-6880/98/05 459-13 $02.00

To average equation (1), the functions φ and $\mathbf{u}$ are presented as sums of their volume averages plus deviations, $\varphi = \bar{\varphi} + \varphi'$ and $u_\alpha = \bar{u}_\alpha + u'_\alpha$, while the impurity fluxes are given by the gradient-like approximation

$$\overline{u'_\alpha \varphi'_i} = -\mu_{\alpha,\beta} \frac{\partial \varphi_i}{\partial x_\beta} \quad (\alpha, \beta = 1, 2, 3). \tag{2}$$

Here, $\mu_{\alpha,\beta}$ is the tensor of diffusion coefficients, and the overbar denotes spatial averaging. We take the tensor principal axes to coincide with the Cartesian coordinate axes, and so we confine ourselves to dealing with diagonal elements only.[13,17,20]

In the equation obtained for deviations, we change coordinates according to the following formula:

$$\sigma = \frac{z - \delta(x, y)}{H - \delta(x, y)} H, \tag{3}$$

where $\delta(x, y)$ describes relief, and H is the upper integration limit.

As a result, the turbulent diffusion equation for the transport of polydisperse aerosol concentrations with the account of coagulation takes the form[9]

$$\frac{\partial \varphi_g}{\partial t} + \operatorname{div} \mathbf{u}\, \varphi_g = I(\varphi_g, x, y, z, t) + \tilde{K}_{ij}(\varphi'_i, \varphi'_j) + F_1 + F_2, \tag{4}$$

where

$$F_1 = \frac{\partial}{\partial x} \mu_{xx} \frac{\partial \varphi_g}{\partial x} + \frac{\partial}{\partial y} \mu_{yy} \frac{\partial \varphi_g}{\partial y} + \frac{\partial}{\partial \sigma} \chi_1 \frac{\partial \varphi_g}{\partial \sigma};$$

$$F_2 = \frac{\partial}{\partial x} a_1 \mu_{xx} \frac{\partial \varphi_g}{\partial \sigma} + a_1 \frac{\partial}{\partial \sigma} \mu_{xx} \frac{\partial \varphi_g}{\partial x} + \frac{\partial}{\partial y} a_2 \mu_{yy} \frac{\partial \varphi_g}{\partial \sigma} + a_2 \frac{\partial}{\partial \sigma} \mu_{yy} \frac{\partial \varphi_g}{\partial y};$$

$$a_1 = \tilde{\delta}_x \frac{\sigma - H}{H - \tilde{\delta}(x, y)}, \tag{5}$$

$$a_2 = \tilde{\delta}_y \frac{\sigma - H}{H - \tilde{\delta}(x, y)}, \quad a_3 = \frac{H}{H - \tilde{\delta}(x, y)};$$

$$\chi_1 = a_1^2 \mu_{xx} + a_2^2 \mu_{yy} + a_3^2 \mu_{\sigma\sigma}.$$

Here φ_g is the concentration vector for particles whose masses are in the interval $(g, g + dg)$; $K_{ij}(\varphi_i, \varphi_j)$ is a matrix operator describing coagulation; $I(x, y, z, t)$ is the source of new particles with size g; and μ_{xx}, μ_{yy}, and $\mu_{\sigma\sigma}$ are the coefficients of turbulent diffusion along x, y, and σ coordinates, respectively.

By using single-point second moments of the turbulent pulsation, the coefficients of turbulent diffusion are determined as functions of the mean atmospheric parameters that is of the shear of air flow, atmospheric stratification, and turbulent energy. The functional dependence of the coefficients of the diffusion tensor on these parameters may be found in Refs. 8, 13, and 17, and it has been used in Refs. 6 and 10. Therefore, here the aerosol particle transport equation (1) with account of coagulation will be solved together with equation of atmospheric hydrothermodynamics.

2.2. Equation of atmospheric hydrothermodynamics

Now we write down the initial system of hydrothermodynamic equations which take the orographic features into account by means of expression (3). In the new coordinate system, the hydrothermodynamic equations in the non-hydrostatic approximation look[1,8,9]

$$\frac{\partial \hat{u}}{\partial t} + \operatorname{div} \mathbf{u}\, \hat{u} = -\frac{\partial P'}{\partial x} + a_1 \frac{\partial P'}{\partial \sigma} + l\, \hat{v}' + F_u + a_3^2 \frac{\partial}{\partial \sigma} \rho \nu_u \frac{\partial}{\partial \sigma} \left(\frac{\hat{u}}{\bar{\rho}} \right), \tag{6}$$

$$\frac{\partial \hat{v}}{\partial t} + \operatorname{div} \mathbf{u}\, \hat{v} = -\frac{\partial P'}{\partial y} + a_2 \frac{\partial P'}{\partial \sigma} - l\, \hat{u}' + F_v + a_3^2 \frac{\partial}{\partial \sigma} \rho \nu_u \frac{\partial}{\partial \sigma} \left(\frac{\hat{v}}{\bar{\rho}} \right), \tag{7}$$

$$\frac{\partial \hat{w}}{\partial t} + \operatorname{div} \mathbf{u}\, \hat{w} = -a_3 \frac{\partial P'}{\partial \sigma} + \lambda \vartheta' (1 + \gamma q) + F_w + a_3^2 \frac{\partial}{\partial \sigma} \rho \nu_u \frac{\partial}{\partial \sigma} \left(\frac{\hat{w}}{\bar{\rho}} \right), \tag{8}$$

$$\frac{\partial \hat{\vartheta}}{\partial t} + \operatorname{div} \mathbf{u}\, \hat{\vartheta} + \frac{S}{a_3} (\hat{w}' + \tilde{\delta}_x \hat{u}' + \tilde{\delta}_y \hat{v}') = \frac{L_w \Phi \bar{\rho}}{C_p} + F_\vartheta + a_3^2 \frac{\partial}{\partial \sigma} \rho \nu_\vartheta \frac{\partial}{\partial \sigma} \left(\frac{\hat{\vartheta}}{\bar{\rho}} \right), \tag{9}$$

$$\frac{\partial \hat{q}}{\partial t} + \operatorname{div} \mathbf{u}\, \hat{q} = -a_3 \hat{w} \frac{\partial Q}{\partial \sigma} - \Phi \bar{\rho} + F_q + a_3^2 \frac{\partial}{\partial \sigma} \rho \nu_q \frac{\partial}{\partial \sigma} \left(\frac{\hat{q}}{\bar{\rho}} \right), \tag{10}$$

$$\frac{\partial \hat{u}'}{\partial x} + \frac{\partial \hat{v}'}{\partial y} + \frac{\partial \hat{w}'}{\partial \sigma} = 0; \tag{11}$$

$u = U + u'$; $v = V + v'$; $w = W + w'$;

$\vartheta = \Theta + \vartheta'$; $q = Q + q'$; $p = P + p'$

(capital letters denote large-scale components of the meteorological fields, and primed letters the deviations). Here we use the notation

$$a_1 = \tilde{\delta}_x \frac{\sigma - \hat{H}}{H - \tilde{\delta}(x, y)}, \quad a_2 = \tilde{\delta}_y \frac{\sigma - \hat{H}}{H - \tilde{\delta}(x, y)},$$

$$a_3 = \frac{\hat{H}}{H - \tilde{\delta}(x, y)};$$

$$\mathrm{div}\ \mathbf{u}\,\hat{\varphi} = \frac{\partial u\hat{\varphi}}{\partial x} + \frac{\partial v\hat{\varphi}}{\partial y} + \frac{\partial w\hat{\varphi}}{\partial \sigma};\quad \hat{\varphi} = \rho\varphi,$$

$$\varphi = (u,\ v,\ w,\ \vartheta',\ q');$$

$$\tilde{\delta}_x = \frac{\partial\tilde{\delta}}{\partial x},\quad \tilde{\delta}_y = \frac{\partial\tilde{\delta}}{\partial y},$$

$$w = a_1\,u + a_2\,v + a_3\,w;$$

$$F_u = \frac{\partial\tau_{11}}{\partial x} + \frac{\partial\tau_{12}}{\partial y} + \frac{\partial}{\partial\sigma}(a_1\,\tau_{11} + a_2\,\tau_{12}), \qquad (12)$$

$$F_v = \frac{\partial\tau_{21}}{\partial x} + \frac{\partial\tau_{22}}{\partial y} + \frac{\partial}{\partial\sigma}(a_1\,\tau_{21} + a_2\,\tau_{22}),$$

$$F_w = \frac{\partial\tau_{31}}{\partial x} + \frac{\partial\tau_{32}}{\partial y} + \frac{\partial}{\partial\sigma}(a_1\,\tau_{31} + a_2\,\tau_{32}),$$

$$F_\vartheta = \frac{\partial H_1}{\partial x} + \frac{\partial H_2}{\partial y} + \frac{\partial}{\partial\sigma}(a_1\,H_1 + a_2\,H_2),$$

$$F_q = \frac{\partial Q_1}{\partial x} + \frac{\partial Q_2}{\partial y} + \frac{\partial}{\partial\sigma}(a_1\,Q_1 + a_2\,Q_2),$$

where t is time; u, v, and w are the wind velocity components along x, y, and σ coordinate axes; $\mathbf{u} = (u, v, w)$, ϑ is the potential temperature; ρ is the density; l is the Coriolis parameter; q is the specific humidity; L_w is the latent heat of condensation, Φ is the rate of transition to liquid phase; S is the stratification parameter; $\lambda = g/T$ is the buoyancy; $\gamma = 0.61$; $\bar{\rho}(z)$ is the background density; τ_{ij}, H_i, and Q_i ($i = 1, 2, 3$; $j = 1, 2$) are the tensor of Reynolds viscid stress, and turbulent heat and moisture fluxes; ν_u, ν_ϑ, and ν_q are the vertical turbulence coefficients for momentum, heat, and moisture moments.

To describe the structure of the near-ground layer, we use the Monin-Obukhov's similarity theory and the empirical Businger's functions.[7,11] As an approximation of the vertical profiles of meteorological fields in the near-ground layer, we assume the "1/3 power law" under the conditions of strong instability, and a linear dependence as described in Refs. 7 and 11 under highly stable conditions. Finally, the model equations for the near-ground layer become

$$æ\,z\,\frac{\partial|\mathbf{u}|}{\partial z} = u_*\,\varphi_u(\zeta),$$

$$æ\,\frac{\partial\tilde{P}}{\partial z} = \tilde{P}_*\,\varphi_\vartheta(\zeta)\quad (P = \vartheta,\ q);$$

$$æ\,|\mathbf{u}| = u_*\,f_u(\zeta, \zeta_u);\ P - P_0 = \tilde{P}_*\,f_\vartheta(\zeta, \zeta_u);$$

$$\zeta = \zeta/L;\ \zeta_h = h/L; \qquad (13)$$

$$\nu_i = \frac{u_*\,æ\,z}{u_i(\zeta)},\ (\nu_i)_h = \frac{u_*\,æ\,H}{\varphi_i(\zeta_h)};$$

$$a_i = \frac{\varphi_i(\zeta)}{f_i(\zeta_h, \zeta_i)};\ L = \frac{u_*^2}{æ^2\,\lambda\varphi_*}\quad (i = u,\ \varphi);$$

$$f_u(\zeta, \zeta_0) = \int_{\zeta_0}^{\zeta}\frac{\varphi_u(\zeta)}{\zeta}\,\mathrm{d}\zeta;$$

$$f_\vartheta(\zeta, \zeta_0) = \int_{\zeta_0}^{\zeta}\frac{\varphi_\vartheta(\zeta)}{\zeta}\,\mathrm{d}\zeta,$$

where $|\mathbf{u}| = (u^2 + v^2)^{1/2}$ is the modulus of the velocity vector; u_* is the friction drag; ϑ_* and q_* are the potential temperature and specific humidity scales; h is the near-ground layer thickness; L is the length scale; z_u and z_ϑ are the roughness parameter for the wind and temperature, ζ is the dimensionless height representing a hydrostatic stability parameter; φ_i and f_i are the directed, universal functions. In the near-ground layer, we will employ potential temperature corrections for the moisture effects that will alter somewhat the length scale L. Therefore, we introduce the length scale $L_* = L\,(J_* + 1)$ and correspondingly the dimensionless height $\zeta^* = z/L_* = \zeta(1 + J_*)$, where $J_* = 0.61\,T(q_h - q_{z_0})/(\vartheta_h - \vartheta_{z_0})$ is the dimensionless number characterizing the relative significance of the effects of humidity and temperature stratifications. We will solve the system of equations (6)–(13) in the domain $D_t = D \times [0, T]$, $D = \{(x, y, \sigma)\colon\ x \in [-X, X],\ y \in [-Y, Y],\ \sigma \in [0, H]\}$ under the following initial and boundary conditions:

$$\hat{u}' + \hat{v}' + \hat{w}' = 0;\ \hat{\vartheta}' = 0;$$

$$\hat{q}' = 0\ \text{ at } t = 0; \qquad (14)$$

$$\frac{\partial\hat{u}'}{\partial x} = \frac{\partial\hat{v}'}{\partial x} = \frac{\partial\hat{w}'}{\partial x} = 0,\ \frac{\partial\hat{\vartheta}'}{\partial x} = 0,$$

$$\frac{\partial\hat{q}'}{\partial x} = 0\ \text{ at } x = \pm X; \qquad (15)$$

$$\frac{\partial\hat{u}'}{\partial y} = \frac{\partial\hat{v}'}{\partial y} = \frac{\partial\hat{w}'}{\partial y} = 0,\ \frac{\partial\hat{\vartheta}'}{\partial y} = 0,$$

$$\frac{\partial\hat{q}'}{\partial y} = 0\ \text{ at }\ y = \pm Y; \qquad (16)$$

$$\hat{u}' = \hat{v}' = \hat{w}' = 0;\ \hat{\vartheta}' = 0;$$

$$\hat{q}' = 0\ \text{ at }\ \sigma = H; \qquad (17)$$

$$a_3\,h\,\frac{\partial\hat{u}}{\partial\sigma} = a_u\,\hat{u},\quad a_3\,h\,\frac{\partial\hat{v}}{\partial\sigma} = a_u\,\hat{v},$$

$$a_3\,h\,\frac{\partial\hat{\vartheta}}{\partial\sigma} = a_\vartheta\,(\hat{\vartheta} - \hat{\vartheta}_0),$$

$$a_3\,h\,\frac{\partial\hat{q}}{\partial\sigma} = a_\vartheta\,(\hat{q} - \hat{q}_0);\quad \frac{\partial\hat{w}}{h} = -\left(\frac{\partial\hat{u}}{\partial x} + \frac{\partial\hat{v}}{\partial y}\right)$$

$$\text{at } \sigma = \frac{(h - \hat{\delta}(x, y))\, \hat{H}}{H - \hat{\delta}(x, y)}; \qquad (18)$$

$$\hat{w}' = 0 \text{ at } \sigma = 0.$$

Surface temperature is determined from the thermal balance equation.

2.3. Parameterization of subgrid-scale turbulent diffusion

Right-hand sides of equations (6)–(13) contain several unknown functions, and below we present semiempirical expressions for their determination. As in Refs. 8 and 12, here we represent the symmetric stress tensor $\tau_{i,j}$ by a function which depends on the deformation tensor D of the mean motion, namely:

$$\tau_{i,j} = \bar{\rho}\, K_M\, D_{i,j}, \qquad (19)$$

where the deformation tensor $D_{i,j}$ and the heat flux H_j are given as

$$D_{i,j} = \frac{\partial u_i}{\partial x_j} + \frac{\partial u_j}{\partial x_i} - \frac{2}{3}\,\delta_{ij}\,\frac{\partial u_k}{\partial x_k} \quad (i = 1, 2;\ j = 1, 2),$$

$$H_j = \bar{\rho}\, K_H\, \frac{\partial \vartheta}{\partial x_j}. \qquad (20)$$

Here K_M and K_H are the parameters of the kinematic viscosity and diffusion ($K_M/K_H = 1/Pr \approx 3$). We define the spatiotemporal variations of the coefficient K_M as

$$K_M = \begin{cases} (\tilde{K}\,\bar{\Delta})^2\ |\mathrm{Def}|, & \text{if } \mathrm{Ri} > 1, \\ (\tilde{K}\bar{\Delta})^2\ |\mathrm{Def}|(1 - (K_H/K_M)\,\mathrm{Ri}), & \text{if } \mathrm{Ri} \le 1, \end{cases} \qquad (21)$$

where $\bar{\Delta} = A^{1/2}$; $A = \Delta x\, \Delta y$; K is the numerical constant. The deformation Def is defined by the formula

$$(\mathrm{Def})^2 = \frac{1}{2}\,\mathrm{Sp}\, D^2 = (D_{11}^2 + D_{22}^2 + D_{33}^2) +$$

$$+ D_{12}^2 + D_{13}^2 + D_{23}^2. \qquad (22)$$

We represent the Richardson number as

$$\mathrm{Ri} = \frac{g}{\Theta}\,\frac{\partial \vartheta}{\partial z} \Big/ (\mathrm{Def})^2.$$

When making numerical calculations for the processes studied that have larger horizontal scales as compared to vertical ones, we use a combined method in which the horizontal coefficients of turbulent exchange are determined from Eqs. (19), (20), and (21), while the vertical ones from the energy balance equations for turbulence and dissipation

$$\frac{\partial b}{\partial t} + \mathbf{u}\,\mathrm{grad}(b) =$$

$$= \nu_u \left[\left(\frac{\partial u}{\partial z}\right)^2 + \left(\frac{\partial v}{\partial z}\right)^2 - \lambda\alpha_T \left(\frac{\partial \vartheta'}{\partial z} + S\right) - \lambda\alpha_q\,\frac{\partial q}{\partial z}\right] +$$

$$+ a_b\,\frac{\partial}{\partial z}\,\nu_u\,\frac{\partial b}{\partial z} - c\,\frac{b^2}{\nu_u}, \qquad (23)$$

$$\frac{\partial \varepsilon}{\partial t} + \mathbf{u}\,\mathrm{grad}(\varepsilon) =$$

$$= \alpha_1\,\frac{\varepsilon}{b}\left[\left(\frac{\partial u}{\partial z}\right)^2 + \left(\frac{\partial v}{\partial z}\right)^2 - \alpha_{\theta_T}\,\frac{\partial \theta'}{\partial z} - \alpha_{\theta_\varepsilon}\,\frac{\partial q}{\partial z}\right] +$$

$$+ \alpha_2\,\frac{\partial}{\partial z}\,\nu\,\frac{\partial \varepsilon}{\partial z} - \alpha_3\,\frac{\varepsilon^2}{b}, \qquad (24)$$

where $\alpha_T = \nu_\vartheta/\nu_u = \varphi_u(\zeta)/\varphi_\vartheta(\zeta)$, a_b and c are the constants.

We will solve these equations with the following initial and boundary conditions[8]:

$$b = 0,\ \varepsilon = 0 \text{ at } t = 0,$$

$$b = b_u^2(\zeta_h, \zeta_0),\ \varepsilon = \varepsilon_h(\zeta_h, \zeta_0) \text{ at } z = h, \qquad (25)$$

$$b = 0,\ \varepsilon = 0 \text{ at } z = H.$$

For definitions of the functions $b_u^2(\zeta_h, \zeta_0)$ and $\varepsilon = \varepsilon_h(\zeta_h, \zeta_0)$ and the methods of their determination, see Ref. 2.

2.4. Coagulation

Normally the transport of aerosol particles in the atmosphere is accompanied by their growth. Time variation of the particle number density and size spectrum is described by the Smolukhovskii equation

$$\frac{\partial \varphi_g}{\partial t} = \frac{1}{2}\int_0^g \tilde{K}(g, g_1)\,\varphi_{g-g_1}\,\varphi_{g_1}\,\mathrm{d}g_1 -$$

$$- \varphi_g \int_0^\infty \tilde{K}(g, g_1)\,\varphi_{g_1}\,\mathrm{d}g_1 + I(\varphi_g, t), \qquad (26)$$

where g_1 is the integration variable (mass); φ_g is the concentration of particles with the mass between g and $g + \mathrm{d}g$; $\tilde{K}(x, y)$ is the collision frequency for particles with masses x and y; $I(\varphi_g, t)$ is the formation rate of particles with the mass g. This last term is added to the right-hand side of equation (1). The first term in expression (26) describes coagulation of smaller-sized particles into those of a bigger size g, while the second one the loss of particles of the size g via coagulation with other particles.

The system of equations (1), (4), and (5) will be solved in the domain

$$D_t = D \times [0, T],$$

$$D = \{(x, y, \sigma) : x \in [-X, X],\ y \in [-Y, Y],$$

$$\sigma \in [0, H]\}$$

under the following initial and boundary conditions:

$$\varphi_g|_{t=0} = \varphi_g^0;$$

$$\frac{\partial \varphi_g}{\partial x} = 0 \quad \text{at} \quad x = \pm X,$$

$$\frac{\partial \varphi_g}{\partial y} = 0 \quad \text{at} \quad y = \pm Y; \tag{27}$$

$$\varphi_g = \varphi_{bg} \quad \text{at} \quad \sigma = H,$$

where φ_{bg} is the background particle concentration.

In the lower integration limit, the boundary condition is given in the parameterized following form:

$$a_3 \frac{\partial \varphi_g}{\partial \sigma} = \frac{a_9 (\tilde{\beta}_g - f_s)}{\tilde{\beta}_g + a_9 \mu_{\sigma\sigma}} \quad \text{at} \quad \sigma = \frac{h - \tilde{\delta}}{H - \tilde{\delta}} H. \tag{28}$$

Here $\tilde{\beta}_g = \beta_g u_* - \omega_g$, β_g characterizes interaction of impurities with the underlying surface; X and Y are the side boundaries of the integration domain over the spatial variables x and y, respectively; $f_g(x, y, t)$, ($g = \overline{1, n}$) describes impurity sources at the roughness level; φ_{gh} is the concentration of aerosol particles at the top of the near-ground layer.

The solution to the problem formulated by expressions (4)–(26) will be sought on the class of nonnegative solutions. The colliding particles are assumed to be spheres and with the size much less than the free path in the ambient gas. Then, $K(x, y)$ can be represented as[18]

$$\tilde{K}(x, y) = A(x^{1/3} + y^{1/3}) (D_x + D_y) \beta_{xy}, \tag{29}$$

where D_x is the diffusion coefficient of a particle with the mass x

$$D_x = \frac{k_B T}{6\pi\eta R_x} \times$$

$$\times \left[1 + Kn_x \left(A + Q \exp\left(-\frac{b_3}{Kn_x}\right)\right)\right]; \tag{30}$$

k_B is the Boltzmann constant; b_3, A, and Q are the empirical constants; $A = 1.25$; $Q = 0.4$; $b_3 = 1.1$. The correction factor β_{xy} is given as[18]

$$\beta_{xy} = \left(\frac{R_x + R_y}{R_x + R_y + d_{xy}} + \frac{4 (D_x + D_y)}{(V_x^2 + V_y^2)^{1/2} (R_x + R_y)}\right)^{-1} \tag{31}$$

$$Kn_x = \frac{l_x}{R_x}; \; d_{xy} = (d_x^2 + d_y^2)^{1/2},$$

$$d_x = \frac{1}{6 R_x l_x} ((2 R_x + l_x)^3 - (4 R_x^2 + l_x^2)^{3/2}) - 2R_x;$$

$$l_x = \frac{8D_x}{\pi V_x}; \quad V_x = \left(\frac{8kT}{\pi x}\right)^{1/2}; \quad x = \frac{4}{3} \pi R_x^3 \rho.$$

Here D_x is the diffusion coefficient of the ith particle with the radius R_x; T is temperature; l_x is the mean free path; V_x is the mean particle velocity; x is the particle mass; ρ is the particle density, and η is the gas viscosity.

3. COMPLEX-CONJUGATE PROBLEM

Environmental protection studies generally focus on achieving global assessments that are functionals of the particle concentration fields rather than of the fields themselves. Among such functionals there are the bulk particle sedimentation rate in a given area, economic damage due to environmental pollution by aerosols and many others. All of them are linearly related to the particle size spectrum. While obtainable directly as described above, more efficiently these variables can be determined using complex-conjugate functions.[4] We shall apply this method to estimate aerosol pollution over Bratsk region and to deduce optimal arrangement of the industrial sources. For simplicity, an impurity is assumed to be passive, that is $K_{ij}(\varphi_i, \varphi_j) = 0$.

Let us write the equation (4) in the operator form as

$$L\varphi = I_g(x, y, z, t), \tag{32}$$

where

$$L\varphi = \frac{\partial \varphi}{\partial t} + \frac{\partial u\varphi}{\partial x} + \frac{\partial v\varphi}{\partial y} + \frac{\partial w\varphi}{\partial \sigma} - F_1 - F_2 \tag{33}$$

and I_g describes pollution sources.

The complex-conjugate operator L^* is defined using the Lagrange identity as

$$(\varphi^*, L\varphi) = (\varphi, L^*\varphi^*). \tag{34}$$

If div $\mathbf{u} = 0$, the complex-conjugate operator is

$$L^*\varphi = -\frac{\partial \varphi^*}{\partial t} - \frac{\partial u\varphi^*}{\partial x} + \frac{\partial v\varphi^*}{\partial y} +$$

$$+ \frac{\partial w\varphi^*}{\partial \sigma} - F_1 - F_2. \tag{35}$$

Now we consider the following complex-conjugate problem:

$$L^*\varphi^* = p_k, \tag{36}$$

where p_k is a nonnegative function of x, y, z, and t; and k belongs to a nonempty set of values. The appropriate boundary conditions are as follows:

$$\frac{\partial \varphi^*}{\partial x} = 0 \text{ at } |x| = X; \tag{37}$$

$$\frac{\partial \varphi^*}{\partial y} = 0 \text{ at } |y| = Y; \tag{38}$$

$$\varphi^* = 0 \text{ at } \sigma = H; \tag{39}$$

$$a_3 \frac{\partial \varphi^*}{\partial \sigma} = \frac{a_\vartheta \beta}{\beta + a_\vartheta \mu_{\sigma\sigma}} \quad \text{at} \quad \sigma = \frac{h - \tilde{\delta}}{H - \tilde{\delta}}; \tag{40}$$

$$\varphi^*(t = T) = 0. \tag{41}$$

In order for the problem, formulated by equations (36) to (41), be properly posed, and for making the numerical algorithm stable, the solution to the problem is sought backward in time: from $t = T$ to $t = 0$. For definiteness, the initial condition is specified for $t = T$. We denote the obtained solution as φ_k^*. Now we multiply the equation (34) by φ^*, integrate it and make a subtraction. Owing to the Lagrange identity, we arrive at a different representation

$$\frac{\partial}{\partial t} (\varphi, \varphi_k^*) = (I, \varphi_k^*) - (p_k, \varphi). \tag{42}$$

Integrating equation (42) over t from $t = 0$ to $t = T$, with the account of the initial conditions for φ_k^* and φ, finally yields

$$\int_0^T \mathrm{d}t \int_D p\varphi \, \mathrm{d}D = \int_D I\varphi^* \, \mathrm{d}D +$$

$$+ \int_0^T \mathrm{d}t \int_{-X}^{+X} \mathrm{d}x \int_{-Y}^{+Y} a_3 \varphi_0 \varphi^* \Big|_{z=h} \, \mathrm{d}y. \tag{43}$$

Here p_k is defined as follows:

$$p_k = \begin{cases} 1, & (x, y, z) \in \omega_k, \\ 0, & (x, y, z) \notin \omega_k, \end{cases} \tag{44}$$

where $\omega_k \subset D$ is the subregion where the total concentration of pollutants is to be estimated (the so-called "monitored area"). It can readily be seen that the left-hand side of equation (43) gives the concentration of pollutants entering ω_k within the time interval $[0, T]$. Thus, the total pollutant concentration in a given part of the D region can be determined by either solving the direct problem, equations (4) to (27), or the complex-conjugate problem, equations (36) to (41). In the latter case, the function φ_k^* describes the fraction of the total pollution amount coming to the.ω_k zone under control.

Some ways of constructing such models for their further use in the environmental monitoring applications are discussed in Refs. 5 and 8.

4. NUMERICAL SOLUTION

Numerical methods for solving equations (4) and (5) have been developed earlier and may be found elsewhere in the literature.[8] Those authors of Ref. 8 present a numerical solution of the hydrodynamic equations (6)–(11) and the transfer equations for the chemically reacting substances that are then included into the right-hand side. From this point of view, the coagulation equation (26) needs nothing new except that its numerical solution is more complicated. Hence some transformations are needed to account for as wide particle size spectrum as possible at a sufficiently low computation costs. For this purpose, the particle size spectrum is introduced as follows.

First we introduce a particle of the ultimately large mass G that, as coagulation progresses, is removed from the system. The reduction in the aerosol particle system mass due to the loss of coarse-fraction particles is small unless the mass of the latter compares with the whole system mass. This can be considered as a natural sink for the system, like that through the gravitational sedimentation of particles.

The entire interval $(0, G)$ was divided into fractions, on the logarithmic scale, by doubling the masses as $2g_i = g_{i+1}$.

The number of particles in the ith fraction, N_i, satisfies the equation that follows from integrating (26) over the mass interval (g_i, g_{i+1}), namely

$$\frac{\partial N_i}{\partial t} = \frac{1}{2} \sum_{j \neq 1}^{i-2} \tilde{K}^1_{i-1,j} N_{i-1,j} N_j + \frac{1}{2} \tilde{K}^0_{i-1,i-1} N^2_{i-1} +$$

$$+ \sum_{j=1}^{i-1} (\tilde{K}^0_{ij} - \tilde{K}^1_{ij}) N_i N_j - \sum_{j=1}^{I} \tilde{K}^0_{ij} N_i N_j, \tag{45}$$

under the initial conditions

$$N_i (t = 0) = N_i^0, \tag{46}$$

where

$$\tilde{K}^1_{ij} = (g_{i+1} - g_i)^{-1} (g_{j+1} - g_j)^{-1} \times$$

$$\times \int_{x+y > g_{i+1}}^{g_{i+1}} \int^{g_{j+1}} \tilde{K}(x, y) \, \mathrm{d}x \, \mathrm{d}y; \tag{47}$$

$$\tilde{K}^0_{ij} = (g_{i+1} - g_i)^{-1} (g_{j+1} - g_j)^{-1} \times$$

$$\times \int_{g_i}^{g_{i+1}} \int_{g_j}^{g_{j+1}} \tilde{K}(x, y) \, \mathrm{d}x \, \mathrm{d}y. \tag{48}$$

When deriving the approximate equation (45), we replaced K values by their mean, over the corresponding mass intervals, values $\tilde{K}$ (Eqs. (46)–(47)).

The right-hand side of the expression (1) may additionally involve source term $I(g, \mathbf{r}, t)$ for new coming arbitrarily shaped particles, as well as the sink term. Let us assume that the particle source produces particles of the most fine fraction. Then it is used to model particle formation due to coagulation.

When applying this model, care should be taken concerning the system mass conservation. The point is that, when mass doubling procedure is used, as it is in our case, and 30 fractions are considered, the mass range of particles involved into the coagulation becomes nine orders of magnitude as wide. Thus, the accuracy of, say, 6 orders of magnitude, while being adequate

when calculating the number concentration, is insufficient for mass concentration calculations, since a small error in the mass concentration of the coarse-fraction particles may grow into a noticeable error in the mass of the entire system. One can avoid these troubles if the initial equation is written for the mass concentrations. One can do this in a similar way by multiplying equation (26) by g and slightly rearranging it, the result being the following evolution equation for the mass concentration:

$$\frac{\partial m_g}{\partial t} = \frac{1}{2}\int_0^g (\tilde{K}^m(g_1, (g-g_1)) +$$

$$+ \tilde{K}((g-g_1), g_1))\, m_{g_1}\, m_{g-g_1}\, \mathrm{d}g_1 -$$

$$- m_g \int_0^\infty \tilde{K}(g, g_1)\, m_g\, \mathrm{d}g_1 , \qquad (49)$$

where

$$g\varphi_g = m_g^0;\ \ \tilde{K}^m(x, y) = \tilde{K}(x, y)\, y^{-1}.$$

Accordingly, the initial condition reduces to

$$m_g|_{t=0} = m_g^0.$$

Next, we integrate both sides of equation (26) over the ith fraction from g to g_{i+1}, remove the averaged product of masses $\bar{m}_i$ and $\bar{m}_j$ out of the integral, and finally obtain that

$$\frac{\partial M_g}{\partial t} = \sum_{j=1}^{i-2} (\tilde{K}_{i-1,j}^{m,1} + \tilde{K}_{j,i-1}^{m,1})\, M_i\, M_j +$$

$$+ \tilde{K}_{i-1,i-1}^{m,0}\, M_{i-1}^2 + \sum_{j=1}^{i-1} (\tilde{K}_{ij}^{m,0} - \tilde{K}_{ij}^{m,1} + \tilde{K}_{ij}^{m,0} -$$

$$- \tilde{K}_{ji}^{m,0})\, M_i\, M_j - \sum_{j=1}^{I} \tilde{K}_{ij}^{m,0}\, M_i\, M_j \qquad (50)$$

with the initial conditions

$$M_i|_{t=0} = M_i^0, \qquad (51)$$

where

$$\tilde{K}_{ij}^1 = (g_{i+1} - g_i)^{-1}\,(g_{j+1} - g_j)^{-1} \times$$

$$\times \int_{x+y>g_{i+1}}^{g_{i+1}} \int^{g_{j+1}} \tilde{K}(x, y)\, y^{-1}\, \mathrm{d}x\, \mathrm{d}y; \qquad (52)$$

$$\tilde{K}_{ij}^0 = (g_{i+1} - g_i)^{-1}\,(g_{j+1} - g_j)^{-1} \times$$

$$\times \int_{g_i}^{g_{i+1}} \int_{g_j}^{g_{j+1}} \tilde{K}(x, y)\, y^{-1}\, \mathrm{d}x\, \mathrm{d}y. \qquad (53)$$

The simplest validity test of the solution just obtained is the conservation of the total system mass. When there are sources and sinks of the aerosol the conservation should hold provided that these sources and sinks are taken into the consideration. Such a validation has been performed in Ref. 3 and showed that the system's particle concentration, in relative units, remains constant accurate to about 10^{-4} (for the particle number) and to 10^{-2} for the mass concentration. Therefore, the numerical scheme can be used for more complex calculations.

The algorithm that is being used for numerically solving this type problems is based on the method of splitting among the physical processes involved, so that, in each short time interval $[t_j, t_{j+1}]$ of the duration Δt, a three-stage scheme is applied. These processes are the transport of aerosol substance along the trajectories, the turbulent diffusion; and the third one is the local change in the aerosol disperse composition due to coagulation. A detailed description of the numerical algorithm and the method of solving the problem using it have been thoroughly discussed elsewhere in the literature.[4,8,9]

We have used the above models in numerical experiments on studying the meteorological processes in the region. The experiments allowed us to estimate the contributions coming from industrial sources of gaseous and aerosol pollution into the air over Bratsk. The idea of the method of numerical experiments is in calculating scenarios most characteristic of the area under study.

The calculations were made for the following values of input parameters: $30 \times 30 \times 15$ number of the region grid nodes used; $X = Y = 72.5$ km; $H = 1550$ m; $\Delta x = \Delta y = 2.5$ km; heights of the coordinate surfaces $z = z_0$, 10, 20, 30, 40, 50, 100, 200, 300, 450, 600, 750, 900, 1100, 1300, and 1500 m; and the time step $\Delta t = 10$ min.

We have estimated the air pollution by aerosol from the sources in Bratsk and in its suburbs. Each source is considered in the model as an aggregated one and sums the contributions from several emission sources. In the emissions, only the number of 10 Å radius particles in the first aerosol fraction is specified, and then their subsequent evolution under the impact of transport, diffusion, and coagulation processes is being simulated. The aerosol pollution sources lie in the plane x, y and have coordinates $x_1 = 27.5$ km, $y_1 = 32.5$ km, $x_2 = 37.5$ km, and $y_2 = 32.5$ km. At these points, the vertical distribution of all sources at heights $z = 10$, 20, 30, 40, and 100 m is taken into consideration. The time used is the local time in Bratsk region. All scenarios start at 06:00 a.m. local time (LT). From the frequency wind rose it follows that prevailing wind direction in this region is from the west, so experiments were taken at the following speeds of the background flow, specified at the 1500 m height: $U_f = 4$ and 0 m/s.

5. EXPERIMENTAL STUDY OF ATMOSPHERIC AEROSOLS

The measurements of atmospheric aerosol concentrations and size spectra were conducted over Bratsk in summer of 1990. The concentrations and disperse composition of atmospheric aerosol were measured with a diffusion aerosol spectrometer.[15] This sampling system consists of the three main components:

1) diffusion batteries that first enlarge the particles to facilitate measurements of size spectra of finely dispersed aerosols (of 0.003 μm size as small).

2) laser aerosol spectrometer, capable of measuring concentration and size spectra of submicron particles (with radii between 0.15 and 3 μm).

3) personal computer that provides for controlling the entire system and accumulating a data bank.

The 4 to 5-min long measurements with the diffusion spectrometer have been carried out, at a certain point where we acquired real-time data. As a result of a single measurement we got information on the total concentration of aerosol particles with radii between 0.003 and 1 μm, the parameters of particle size distribution (mean radius and size distribution width for finely-dispersed aerosol particles with radii up to 0.1 μm, and the concentration and size distribution histogram of submicron particles with the radii from 0.15 to 2.0 μm, binned in 10 intervals: (≤ 0.15 μm), (0.15–0.2), (0.2–0.3), (0.3–0.4), (0.4–0.5), (0.5–0.7), (0.7–1.0), (1.0–1.5), (1.5–2.0), (≥ 2.0 μm).

This information was saved together with the date and time of measurements accurate to one minute. These data have been stored in the computer, so they can subsequently be processed in a desired way. Principles of operation of our experimental setup have been well described elsewhere.[16] Sampled atmospheric air is blown through the diffusion batteries together with aerosol particles, whose trapping by the battery, defined as the ratio of particle concentrations before and after the passage through the battery, depends on the particle size distribution. Thus, the quantities actually measured in the experiment are the amounts of particles trapped by the batteries. To extract useful information on aerosol particle size distribution, it is necessary to additionally solve an inverse problem, that is to solve an integral equation of the first kind. Parameters of the size distribution of finely dispersed particles were determined in the course of simplified inversion procedure as described in Ref. 16.

As part of the experiment, we continuously sampled aerosol particles in the free atmosphere; for which purpose, we selected 5 points, where the measurements have been continuously conducted for several days. As a result, a data bank was accumulated for five points. In each measurement, we have been determining particle size distribution (approximated by the gamma distribution) and the total particle concentration. For submicron particles a more exact size distribution has been determined as well. With about 4 min duration of a single measurement, a total of 250 to 300 experimental data points per day have been acquired. The measurement results were processed to retrieve the time behavior of the total particle concentration, time variation of the submicron particle concentration, and the distribution of concentrations at a given observation point.

Here we did not directly compare experimental results with numerical calculations. We rather use the experimental data to illustrate the theoretical calculations and to calibrate them. The reason was in the absence of accurate data on the emission rates and aerosol distributions. So, we varied emission rates to obtain a qualitative agreement between the numerical model results and the experimental data available. A more detailed comparison between these results will be done in a future work.

6. DISCUSSION OF RESULTS

6.1. Results of numerical calculations

To study the meteorological situations and for estimating the role of the emission sources on aerosol and gaseous air pollution in Bratsk, we have carried out a number of numerical experiments.

To illustrate the calculated results on the scenarios by the above-mentioned models, two types of figures were prepared. Figures of first type (1 through 3) present two-dimensional transects of the flow fields and contour plots of the aerosol concentration for the eighth fraction, of the 0.256 μm size (t = 14:00 LT, z = 10, 50, 450 m, left-hand side of the figure). Shown in the right-hand sides of the figures are the diameter distributions (histograms) for aerosol particles formed at different distances from the source (circled numbers 1 through 4) and at different altitudes above the Earth's surface. As seen from Figs. 1 to 3, nonlinearity of the coagulation process results in different particle size spectra at different points. As a consequence, this, in turn, leads to an essentially unsteady of processes the aerosol formation at different distances from the source and, hence, to a strong spatial variability in the particle sedimentation.

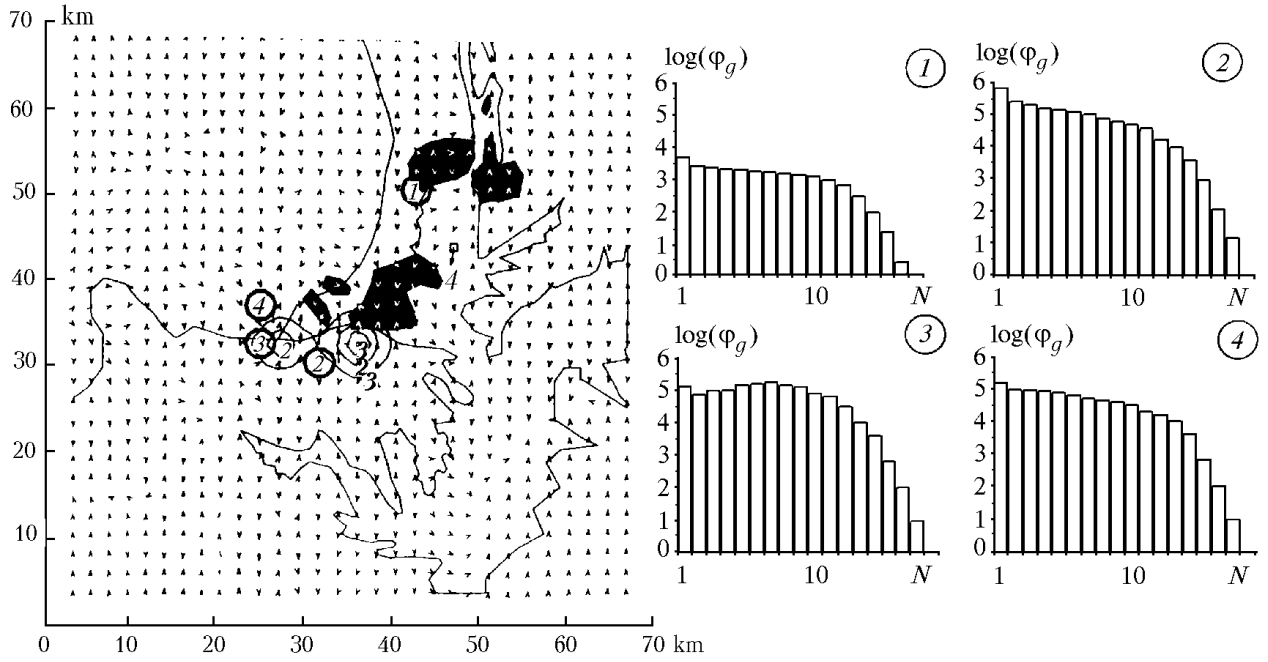

FIG. 1. Two-dimensional transects of the air flow field (without the background flow) and contours of aerosol concentration for the eighth fraction, that corresponds to 0.256 μm, t = 14:00 LT, z = 10 m *(left-hand side). Contour lines numbered 1 through 5 correspond to the following values* (particles per cm^3): $1.22 \cdot 10^5$ *(1),* $2.44 \cdot 10^5$ *(2),* $3.51 \cdot 10^5$ *(3),* $4.89 \cdot 10^5$ *(4), and* $6.11 \cdot 10^5$ *(5). Diameter distributions (histograms) of aerosol particles, formed at different distances from the emission source (circled numbers 1–4) and at different heights above the surface (right-hand side). Shown in dark is the region located within the urban area of Bratsk-city.*

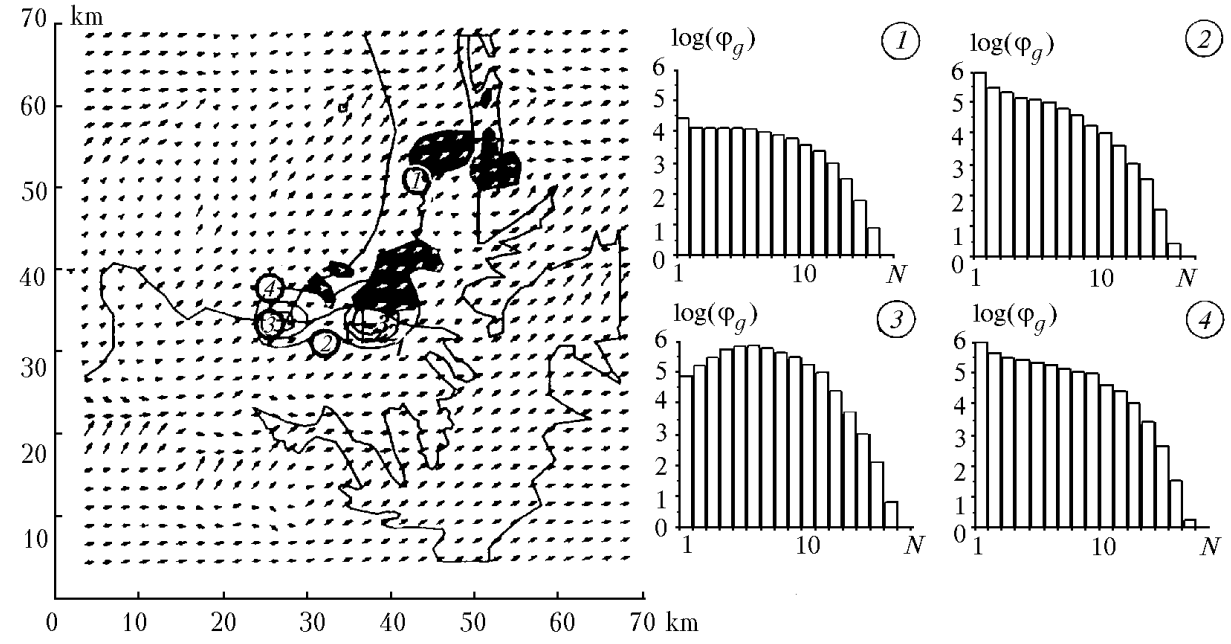

FIG. 2. Same as in Fig. 1, but for z = 50 m *and the flow speed of* 4 m/s. *Contour lines numbered 1 through 5 correspond to the following values* (particles per cm^3): $1.18 \cdot 10^5$ *(1),* $2.35 \cdot 10^5$ *(2),* $3.51 \cdot 10^5$ *(3),* $4.71 \cdot 10^5$ *(4), and* $5.88 \cdot 10^5$ *(5).*

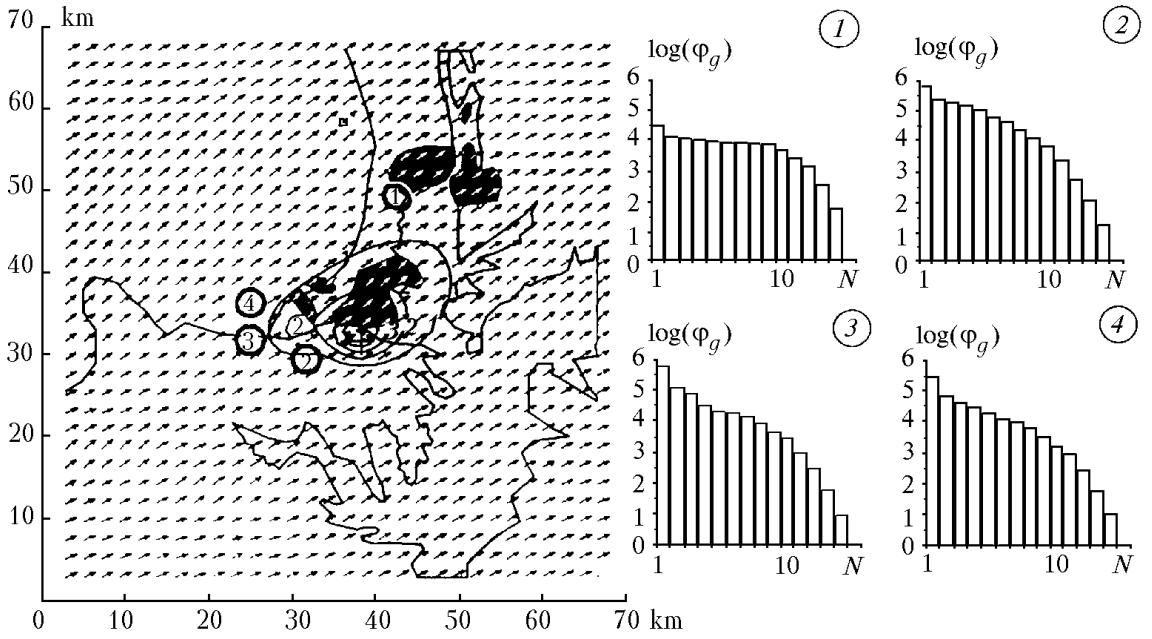

FIG. 3. Same as in Fig. 2, but for $z = 450$ m. *Contour lines numbered 1 through 5 correspond to the following values (*particles per cm^3*):* $4.93 \cdot 10^4$ *(1),* $9.85 \cdot 10^4$ *(2),* $1.48 \cdot 10^5$ *(3),* $1.97 \cdot 10^5$ *(4), and* $2.46 \cdot 10^5$ *(5).*

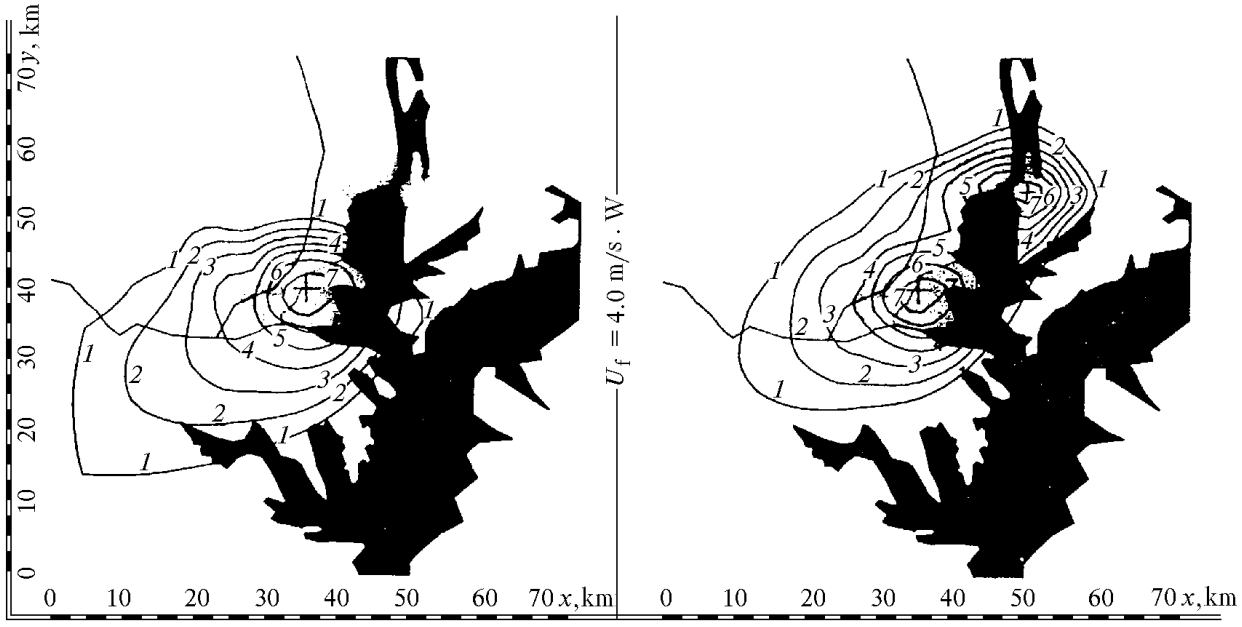

2.602 3.469
2.891 3.758
3.180 4.047
4.336

1.858 2.477
2.064 2.683
2.270 2.890
3.096

FIG. 4. Danger functions φ^* *for different zones under control (marked by crosses) of the Bratsk region: one protected zone (left-hand side,* $\varphi^*_{max} = 2.89 \cdot 10^{-7}$*) and two protected zones (right-hand side,* $\varphi^*_{max} = 2.06 \cdot 10^{-7}$*). Zones of highest danger are outlined by the contour lines numbered by 7 (on the logarithmic scale). Shown in dark is the region located within the urban area of Bratsk-city.*

The second type of figures presents two-dimensional transects of the fields of the pollution danger function for Bratsk-city, calculated with the account of contribution from neighboring populated centers. The larger the contour line number the larger is the contribution from the emission sources, located in the corresponding parts of the region, to air pollution of the Bratsk-city and of the localities around it. Most dangerous regions are those outlined with line number *7* (on the logarithmic scale). The relative contributions of the sources to air pollution in Bratsk have weights between 100 and 10%. The region encompassed by contour lines, numbered *7* and *6*, corresponds to 10 to 1% relative contribution to pollution of the lower 150-m-thick layer. The region between *6* and *5* contour lines corresponds to 1 to 0.1% contribution, etc.

As analysis shows, the danger functions for the pollution sources in the urban atmosphere strongly depend on the direction and intensity of the background flow, as well as on local circulation, formed under the impact of this flow. As wind velocity increases and changes its direction, the region affected by the emissions grows accordingly in size and changes in shape (Fig. 4). As numerical experiments and field studies demonstrate, aerosol concentration may vary by an order of magnitude, during the period of a day as short, owing to diurnal variation of the atmospheric processes. Thus, we see from what have been discussed, that even at a constant-level atmospheric emissions independent of the current atmospheric conditions, the permissible levels of atmospheric pollution can hardly be achieved with the industrial technologies that exist now in Bratsk. Creating of improved environmental control systems that are based on the health-ecology standards and ecological criteria is needed.

6.2. Measurement results

Figures 5*a–d* show the diurnal behavior of the concentrations of finely dispersed and submicron aerosol fractions. Quite distinct is the day-to-night change in aerosol concentration; which is characteristic of urban aerosols, and is a result of increased anthropogenic activity during day-time and, possibly, some atmospheric processes of photochemical gas-to-particle conversions.

Additionally, we have analyzed the spatial distributions of concentration of the submicron and finely dispersed aerosols. In particular, we have calculated the probability of occurrence of some aerosol concentrations at a given location. This analysis enables revealing which regions contribute to aerosol overburden of a given location, and provides for estimating air quality in this place. One such distribution is depicted in Fig. 6.

From the figure we see that, while moving into the plume, the percentage of large concentrations rapidly increases, that is the mode of the concentration distribution shifts towards larger values. Under the background conditions, the probability of occurrence for the concentration either has a peak at smaller values or monotonically decreases with increasing concentration without any peaks.

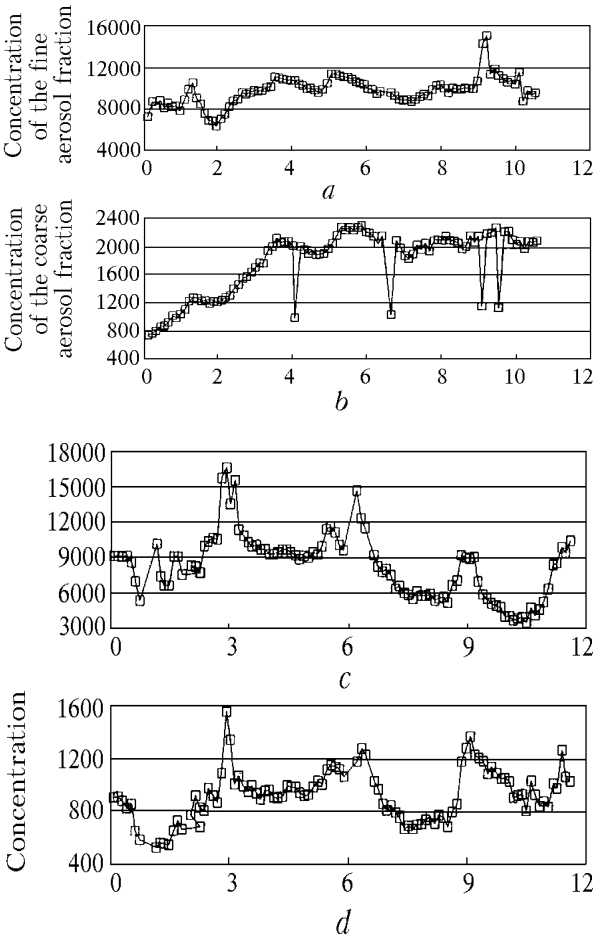

FIG. 5. Time behavior of the fine (a) and coarse (b) aerosol fraction measured on July 10, 1990, the same on July 9, 1990 (c, d).

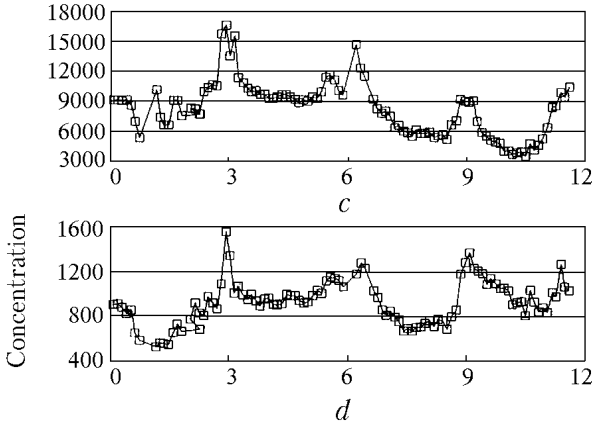

FIG. 6. Distribution of aerosol concentrations for polluted zone of Bratsk-city on July 10, 1990.

6.3. Comparison of the numerical and measurement results

It is interesting to make a comparison between the theoretical and experimental data obtained. This comparison, however, must be regarded merely as an estimate. The first reason for this is that the meteorological situations can never be reproduced and also because measurements at a single point are random in nature, whereas the simulations were performed within a deterministic framework. Besides, the simulations made did not allowance for the background level of the earlier existing aerosol and as well as for the prior transport of atmospheric air from neighboring regions. Therefore, such a comparison was used here simply to estimate the emission rates of aerosol sources, specifically, the source powers were tuned so as to obtain matching between the experimental and theoretical levels of particle concentration and size spectra.

Such normalization can be considered by an example of plume from the Bratsk timber plant that was flowing toward the region of Bratsk hydroelectric power station. The appearance of this plume may be seen in Fig. 5.

It should be noted that finely dispersed aerosol fraction was found to be more sensitive, i.e., faster responding, to pollution than the submicron one, as is obvious from Figs. 5*a* and *b*. In 4–6 hour, the concentration of finely dispersed aerosol fraction has already reached its steady-state level (Fig. 5*a*), whereas the submicron fraction only began to respond to this concentration change (Fig. 5*b*).

As a result, in such situations the calculations give full concentration of aerosol particles ($N_{max} = 10^5$ cm^{-3}), while the measured values are an order of magnitude lower. This led us to a conclusion that assumed source power might have been overestimated by as much as a factor of three. Subsequent comparisons with measurements conducted nearby the source confirmed this.

7. CONCLUSIONS

In this paper we have presented some results that demonstrate the potentialities of mathematical models in applications to solving some problems in the environmental protection. Although being quite sophisticated, they could be an effective tool for predicting consequences of aerosol emissions of both anthropogenic and natural origin. One such model, based on a limited set of aerosol transformation processes, has been used here and gave realistic results on the atmospheric aerosol characteristics needed.

The measurement data obtained during the summer mission in 1990 as well as the simulations of aerosol pollution of the atmospheric over Bratsk have shown that:

1) The Bratsk water storage basin forms a well detectable microclimatic system. Complex orography and nonuniformity of the surface heating result in a complicated local air circulation.

2) The concentration of finely-dispersed (0.05 μm) aerosol (10^4–10^6 cm^{-3}) exceeds the background level by one to two orders of magnitude, while that of the submicron (0.05–2.0 μm) aerosol ranges from 10^2 to 10^4 cm^{-3}, that is several order of magnitude above the background level.

3) Using the spatiotemporal structure of solutions of the conjugate problem, it is possible to detect locations of sources contributing to pollution of a given area.

4) Good agreement between the measured and simulated diurnal behavior of aerosol concentrations shows that the model can successfully be used to estimate the power of pollution sources. The pollution rate for Bratsk-city was found to be 10^8 cm^{3}s^{-1}.

Finally, we have determined the aerosol particle size distribution functions for some parts of Bratsk. They characterize levels of air pollution near a source and at different distances from it.

ACKNOWLEDGMENT

The work was partially supported by the Russian Foundation for Basic Researches (grant No. 96–05–64733).

REFERENCES

1. A.E. Aloyan, "*Non-hydrostatic numerical models of local atmospheric processes*,B Preprint No. 817, Computer Center of Siberian Branch of the Academy of Sciences of the USSR, Novosibirsk (1984), 41 pp.

2. A.E. Aloyan and G.L. Lazriev, in: *Mathematical Models of Atmospheric Motion* (Novosibirsk, 1980).

3. A.A. Lushnikov and V.N. Piskunov, Dokl. Akad. Nauk SSSR **268**, No. 1, 132–136 (1982).

4. G.I. Marchuk, *Mathematical Simulation in the Environmental Protection Problem* (Nauka, Moscow, 1982).

5. G.I. Marchuk and A.E. Aloyan, "*Mathematical simulation in ecological problems*,B Preprint No. 234, OVM of the Academy of Sciences of the USSR, Moscow (1989), 36 pp.

6. G.I. Marchuk, A.E. Aloyan, A.A. Lushnikov, and V.A. Zagainov, "*Mathematical simulation of transport of atmospheric aerosol with the account of coagulation*,B Preprint No. 247, OVM of the Academy of Sciences of the USSR, Moscow (1990), 30 pp.

7. A.S. Monin and A.M. Yaglom, *Statistical Hydromechanics* (Nauka, Moscow, 1965), 640 pp.

8. V.V. Penenko and A.E. Aloyan, *Models and Methods in Environmental Protection Problems* (Nauka, Moscow, 1985).

9. A.E. Aloyan, A.A. Lushnikov, S.V. Makarenko, G.I. Marchuk, and V.A. Zagainov, Russian Journal of Numerical and Analytical Mathematical Modeling,

No. 8, 17–30 (1993).
10. A.E. Aloyan, V.O. Arutyunyan, and G.I. Marchuk, Russian Journal of Numerical and Analytical Mathematical Modeling, No. 10, 93–114 (1995).
11. J.A. Businger, I.C. Wyngard, Y. Izumi, and E.F. Bradley, J. Atmos. Sci., No. 28, 181 (1971) .
12. T. Gal-Chen and C.J. Sommerville, J. Comp. Phys., No. 17, 276 (1975).
13. B.E. Freman, J. Atmos. Sci. **34**, No. 1, 124–136 (1977).
14. W.S. Lewellen and M.E. Teske, Boundary Layer Meteorology **10**, 69–90 (1976).
15. A.A. Lushnikov and V.A. Zagainov, J. Aerosol Sci., No. 20, 987 (1989).
16. A.A. Lushnikov, Yu.V. Julanov, and V.A. Zagayinov, J. Aerosol Sci., No. 25, 533 (1993).
17. G.L. Mellor and T. Yamada, J. Atmos. Sci. **31**, 1791 (1974).
18. S.H. Suck and J.R. Brock, J. Aerosol Sci. **10**, 581–590 (1979).
19. T. Yamada and S. Bunker, J. Appl. Meteorol. **27**, No. 5, 562–578 (1988).
20. D.L. Yordanov and A.E. Aloyan, Comptes. Rend. Acad. Bulgar. Sci. **34**, No. 7, 981–983 (1981).